# Dual quantum cascade laser-based sensor for simultaneous NO and NO$_2$ detection using a wavelength modulation-division multiplexing technique

Yajun Yu[1,2] · Nancy P. Sanchez[3] · Fan Yi[1] · Chuantao Zheng[2] · Weilin Ye[2] · Hongpeng Wu[2] · Robert J. Griffin[3] · Frank K. Tittel[2]
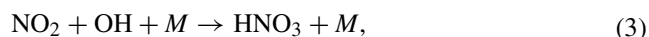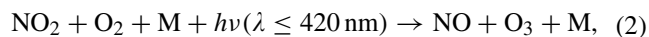
**Abstract** A sensor system capable of simultaneous measurements of NO and NO$_2$ was developed using a wavelength modulation-division multiplexing (WMDM) scheme and multi-pass absorption spectroscopy. A continuous wave (CW), distributed-feedback (DFB) quantum cascade laser (QCL) and a CW external-cavity (EC) QCL were employed for targeting a NO absorption doublet at 1900.075 cm$^{-1}$ and a NO$_2$ absorption line at 1630.33 cm$^{-1}$, respectively. Simultaneous detection was realized by modulating both QCLs independently at different frequencies and demodulating the detector signals with LabView-programmed lock-in amplifiers. The sensor operated at a reduced pressure of 40 Torr and a data sampling rate of 1 Hz. An Allan–Werle deviation analysis indicated that the minimum detection limits of NO and NO$_2$ can reach sub-ppbv concentration levels with averaging times of 100 and 200 s, respectively.

## 1 Introduction

Nitrogen oxides (NO$_x$), including nitric oxide (NO) and nitrogen dioxide (NO$_2$), have been identified as prominent atmospheric pollutants, playing important roles in controlling the photochemical production of tropospheric ozone (O$_3$), determining the concentration of the hydroxyl radical (OH) and contributing to the formation of secondary organic aerosols as well as acid precipitation [1–4]. The transformational relations of atmospheric NO$_x$, O$_3$ and OH are principally given by the following reactions [5]:

$$NO + O_3 \rightarrow NO_2 + O_2, \tag{1}$$

$$NO_2 + O_2 + M + h\nu(\lambda \leq 420\,nm) \rightarrow NO + O_3 + M, \tag{2}$$

$$NO_2 + OH + M \rightarrow HNO_3 + M, \tag{3}$$

where $M$ represents an inert molecule that absorbs excess molecular energies. Over the past century, global anthropogenic NO$_x$ emissions have increased drastically as a result of fossil fuel combustion and biomass burning, which significantly impacts human health and atmospheric chemistry [5, 6]. Therefore, the ability to perform sensitive and selective NO$_x$ measurements is critical for environmental monitoring and climate research.

The conventional method for the determination of ambient NO$_x$ concentration levels is chemiluminescence [3, 7, 8]. This technique allows direct NO detection and indirect NO$_2$ quantification by the catalytic or photolytic conversion of NO$_2$ to NO, followed by an ozone-induced chemiluminescent reaction with NO. However, the conversion of NO$_2$ to NO can lead to sampling artifacts and interference from other ambient nitrogen-containing compounds, resulting in unreliable NO$_2$ quantification [9]. Laser-based absorption techniques provide precise, fast-responsive, and non-invasive sensing capabilities that make it feasible to perform the measurements of NO and NO$_2$ alternatively and simultaneously.

Some laser-based in situ measurements of NO or NO$_2$ have been implemented for pollution studies, such as vehicle emission [10], combustion processes [11–13] and industrial exhaust [14]. In these cases, in situ

✉ Yajun Yu
  yu_yj@whu.edu.cn; yjy@rice.edu

1  School of Electronic Information, Wuhan University, Wuhan 430072, China

2  Department of Electrical and Computer Engineering, Rice University, 6100 Main Street, Houston, TX 77005, USA

3  Department of Civil and Environmental Engineering, Rice University, 6100 Main Street, Houston, TX 77005, USA

analyses of pollutant species were conducted at atmospheric pressure. The spectral absorption lines of interest were widely pressure broadened and easily subjected to interference from other species. In addition, these sensor systems operated in harsh environments with low detection sensitivities of ~ppmv levels. For applications in ambient atmospheric monitoring, high sensing precision and sensitivity are needed for measuring $NO_x$ at low concentrations of ~ppbv levels [6, 15]. Long effective optical path-length spectroscopy [16], including multi-pass absorption spectroscopy and cavity-enhanced absorption spectroscopy, is a useful tool to improve the trace gas sensor performance by lowering the sampling pressure and increasing the effective optical absorption path-length.

Several optical sensing techniques using long effective optical path-length spectroscopy have been employed for NO [15, 17, 18] and $NO_2$ [19–21] detection separately. Simultaneous measurements of atmospheric $NO_2$ and $NO_x$ were realized by a double-channel cavity ring-down spectroscopy (CRDS) instrument at 404 nm [22]. $NO_2$ was directly detected in one channel and $NO_x$ was detected in a second channel by quantitative conversion of ambient NO into $NO_2$ in excess $O_3$. A spectrometer based on two time-division multiplexed, continuous wave (CW) quantum cascade lasers (QCLs) emitting at ~1600 and 1900 $cm^{-1}$, respectively, able to perform direct absorption spectroscopic (DAS) measurements of tropospheric NO and $NO_2$ with a multi-pass gas cell (MPGC) of 204 m optical path-length was reported [8]. A pulsed mode, dual-wavelength QCL with electrically separated distributed-feedback (DFB) sections was demonstrated to probe NO at 1890.71 $cm^{-1}$ and $NO_2$ at 1599.14 $cm^{-1}$ simultaneously [23]. However, the QCL was mismatched to the best-suited absorption features.

In this paper, we report the development of a dual QCL based sensor system for simultaneous detection of the two most common atmospheric nitrogen oxides, i.e., NO and $NO_2$, using an astigmatic Herriott MPGC with an effective optical path-length of 76 m. A wavelength modulation-division multiplexing (WMDM) strategy [24] was implemented to achieve the simultaneous monitoring via modulating each QCL at a different frequency and demodulating the detector signal with custom-made LabView-based lock-in amplifiers. Optimum target absorption lines determined by means of HITRAN simulations with the conditions of a pressure of 40 Torr and a temperature of 296 K were selected to perform the $NO_x$ measurements at sub-ppbv concentration levels.

## 2 Sensor design

### 2.1 Experimental configuration

The sensor configuration is schematically depicted in Fig. 1. A thermoelectrically cooled (TEC), CW DFB-QCL (Hamamatsu Photonics, LE0178) emitting at ~5.26 μm was utilized as the excitation source for NO detection. The laser temperature (19.5 °C) and injection current (657 mA) were controlled by a temperature controller (Thorlabs, TED200C) and a current source (ILX Lightwave, LDX-3232), respectively. The combined waveform of wavelength sinusoidal tuning (1 Hz, 8 mA) and modulation (40 kHz) was generated by an analog output from a LabView-controlled data-acquisition (DAQ) card (National Instruments, USB-6361) and supplied to the QCL current source to realize wavelength modulation. Furthermore, a water-cooled, CW external-cavity (EC) QCL (Daylight Solutions, Model 21062-MHF) with a spectral tuning range from 1535 to 1640 $cm^{-1}$ was operated by a laser controller (Daylight Solutions, Model 1001-TLC) to set the EC-QCL chip current at 515 mA and emitting wavenumber at ~1630 $cm^{-1}$ for $NO_2$ detection. A low-frequency sinusoidal waveform (1 Hz, 175 mV) was produced by a combination of a function generator (Tektronix, AFG 3102) and a PZT driver (Thorlabs, MDT691) to scan the EC-QCL wavelength. A high-frequency (19 kHz) modulation waveform generated from another analog output of the DAQ card was added to the injection current. Detailed description of the EC-QCL characterization and operation can be found elsewhere [13, 25–27]. The DAQ card was triggered by the function generator to synchronize the entire signal processing system. Figure 2 shows a time sequence of the DFB-QCL and EC-QCL scanning signals produced by a current source and a function generator, respectively, in a scanning period of 1 s. The data-acquisition time was used to tune the wavelengths of QCLs, and collect detector signals with the DAQ card, while the data processing time was occupied to process and save data by a LabView program installed in a laptop. The DFB-QCL output was collimated by a high NA = 0.56 antireflection coated aspheric lens (Thorlabs, C028TME-E) with a focal length of 5.95 mm. The EC-QCL output beam quality was optimized by passing the beam through a spatial filter consisting of two $CaF_2$ plano-convex lenses (with focal lengths of 40 and 50 mm, respectively) and a pinhole (with a diameter of 400 μm). A pair of beam splitters separated each laser beam into two different optical
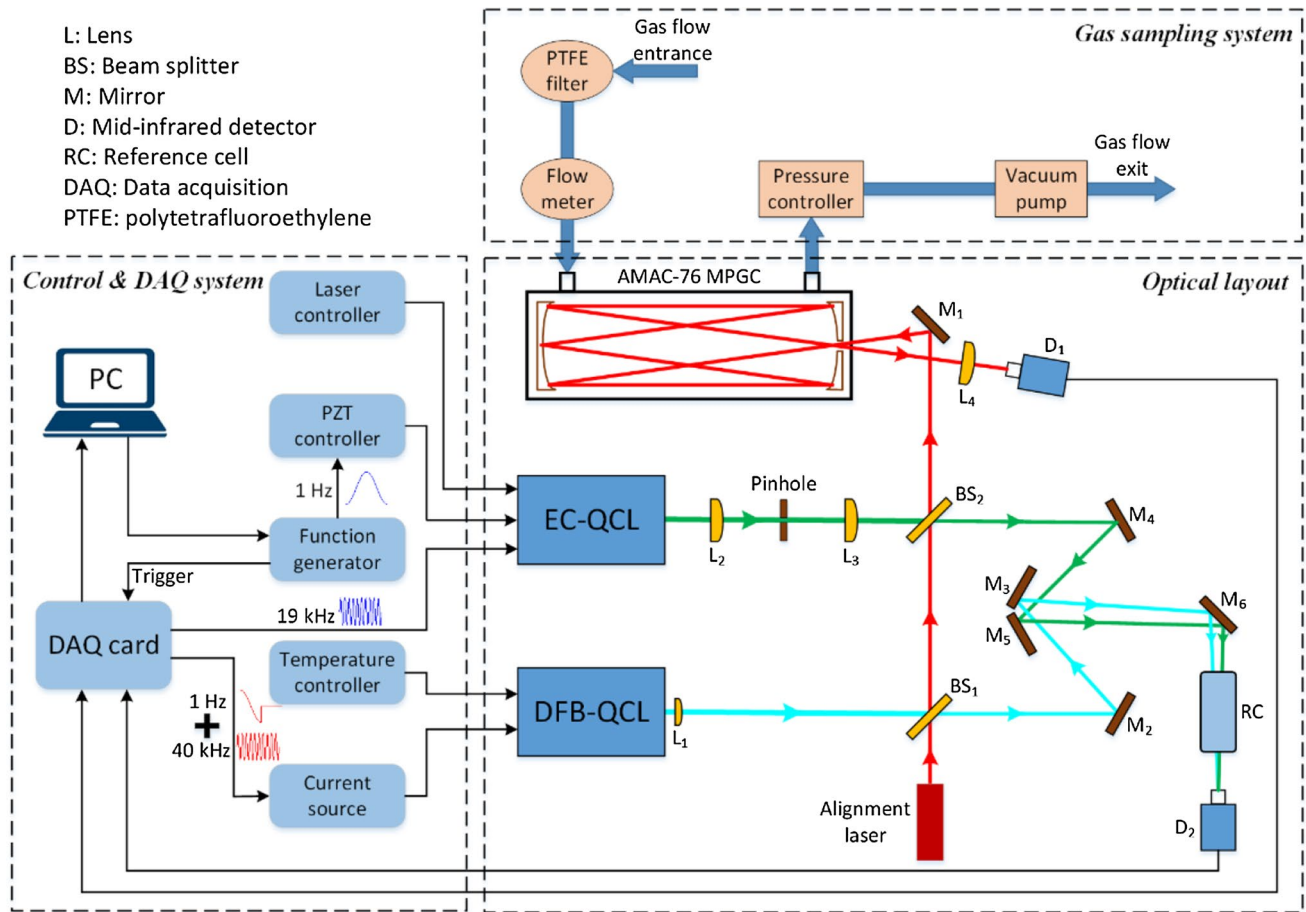
**Fig. 1** Schematic diagram of a dual QCL based sensor system for simultaneous NO and NO$_2$ detection
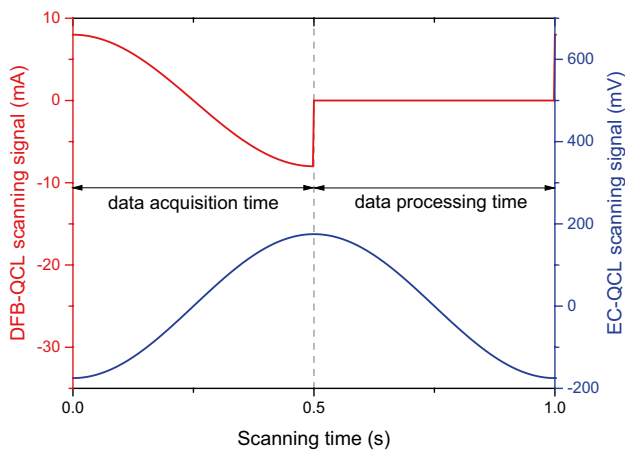


**Fig. 2** A time sequence of DFB-QCL (in *red*) and EC-QCL (in *blue*) scanning signals generated by the DAQ card and the function generator, respectively, in a 1-s scanning period

paths, one as the main beam for the gas sample and the other as the reference beam for wavelength locking. The main beam, co-aligned with a visible alignment laser (coherent, $\lambda = 630$ nm) for beam tracing purposes, was coupled into a 76 m astigmatic Herriott MPGC (Aerodyne Research Inc., AMAC-76). The beam exiting the MPGC was focused onto a TEC mercury-cadmium-telluride (MCT) detector (Vigo Systems, PVMI-3TE-8) with a 40-mm focal length plano-convex lens. The reference beam of each laser was directed through a reference gas cell by five mirrors (see M$_2$, M$_3$, M$_4$, M$_5$ and M$_6$ in Fig. 1) and subsequently collected by a second mid-infrared detector (Vigo Systems, PVM-10.6). The reference cell was filled with high concentration samples of NO and NO$_2$ at a pressure of ~30 Torr. The electrical signals of the main and reference beams were acquired by the DAQ card and then demodulated to extract the corresponding

second-harmonic (2*f*) components for gas concentration monitoring and third-harmonic (3*f*) components for wavelength locking, respectively, using custom-made LabView-programmed lock-in amplifiers in a laptop. In the gas sampling system, a polytetrafluoroethylene filter (Pall Corporation, pore size 2.0 μm) for dust retention and a flow meter (Alicat Scientific, M-2SLPM-D/5M) were connected to the inlet of the MPGC. The system pressure was maintained at 40 Torr by a pressure controller (MKS Instruments, Type 640) and an oil-free vacuum pump (Varian, DS102) downstream to the MPGC. The low sampling pressure of 40 Torr can reduce absorption linewidth and eliminate possible interferential absorption overlap, which will be discussed in detail in Sect. 2.2.

## 2.2 Selection of absorption lines

Selection of the optimum target absorption lines for NO and $NO_2$ was carried out by comprehensive examination of the HITRAN database [28]. The NO molecule has a strong fundamental vibrational band near $\lambda = 5.2$ μm with an intense NO $R$(6.5) absorption doublet, which is a superposition of six lambda coupling components centered at 1900.075 $cm^{-1}$. Figure 3a shows transmission spectra of 20 ppb NO and standard air (with a mixture of 1.2% water vapor, 380 ppm $CO_2$, 2 ppm $CH_4$, 320 ppb $N_2O$ and 10 ppb $NH_3$) in the spectral region from 1899.5 to 1900.5 $cm^{-1}$. The simulated conditions were at a gas pressure of 40 Torr, a temperature of 296 K and an optical path-length of 76 m. The NO absorption doublet at 1900.075 $cm^{-1}$ is free from interference of other atmospheric species due to a flat absorption background. The peak $NO_2$ absorption in the $R$-branch of fundamental

$v_3$ vibration occurs at 1630.33 $cm^{-1}$. As plotted in Fig. 3b, the well resolved $NO_2$ line at 1630.33 $cm^{-1}$ is quasi-interference-free, with the same conditions of Fig. 3a described above, in the spectral range of 1629.8–1630.8 $cm^{-1}$. Note that the strong absorption background of standard air in Fig. 3b is mainly caused by several intense adjacent water lines. The selected absorptions of NO at 1900.075 $cm^{-1}$ and $NO_2$ at 1630.33 $cm^{-1}$ are covered by spectral tuning ranges of the DFB-QCL and EC-QCL, respectively.

## 2.3 Determination of dual QCL tuning rates

To determine the laser frequency tuning rates, the reference cell in the experimental setup was replaced by a germanium etalon (Team Photon, with a free spectral range of 0.0164 $cm^{-1}$), which results in the "etalon" fringes of both QCL intensities as shown in the upper panels of Fig. 4a, b. The intensity signals were recorded with 400 thousand sampling points in each data-acquisition period. The peak positions of the fringes were extracted and fitted using sinusoidal functions to characterize the relative wavenumber variations depicted in the lower panels of Fig. 4a, b. The fittings provided coefficients of determination ($R^2$) of 0.99987 and 0.99999, indicating an excellent sinusoidal relationship between the relative wavenumber and the sampling points. Hence the absolute wavenumber corresponding to each sampling point can be retrieved via the fitted sinusoidal function once a real wavenumber value of one sampling point is determined. Note that the DFB-QCL intensity signal (Fig. 4a, upper panel) at beginning sampling points was distorted mainly due to the rising edge of the scanning waveform generated from the DAQ card (see Fig. 2).
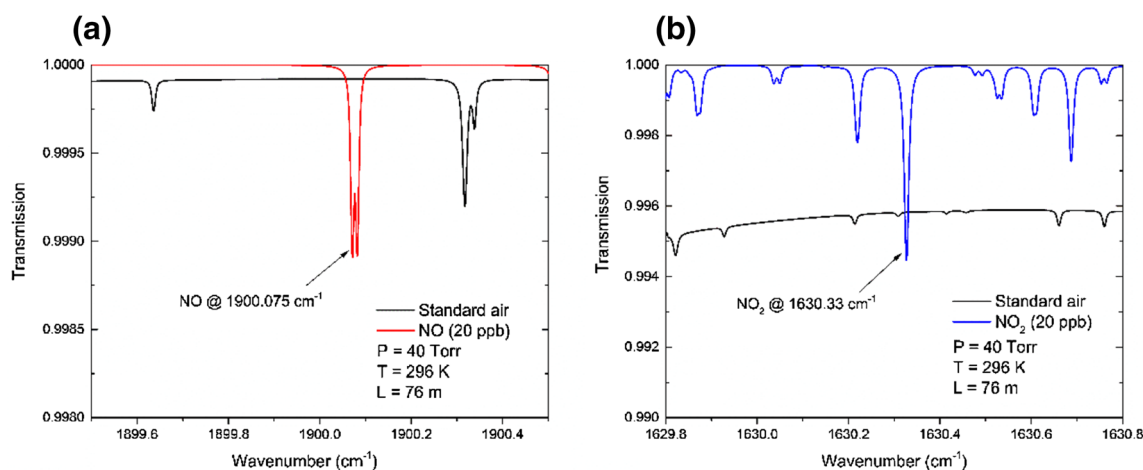


**Fig. 3** HITRAN simulation for transmission spectra of **a** 20 ppb NO and **b** 20 ppb $NO_2$ with standard air (1.2% water vapor, 380 ppm $CO_2$, 2 ppm $CH_4$, 320 ppb $N_2O$ and 10 ppb $NH_3$) at 40 Torr, 296 K and a 76-m optical path-length
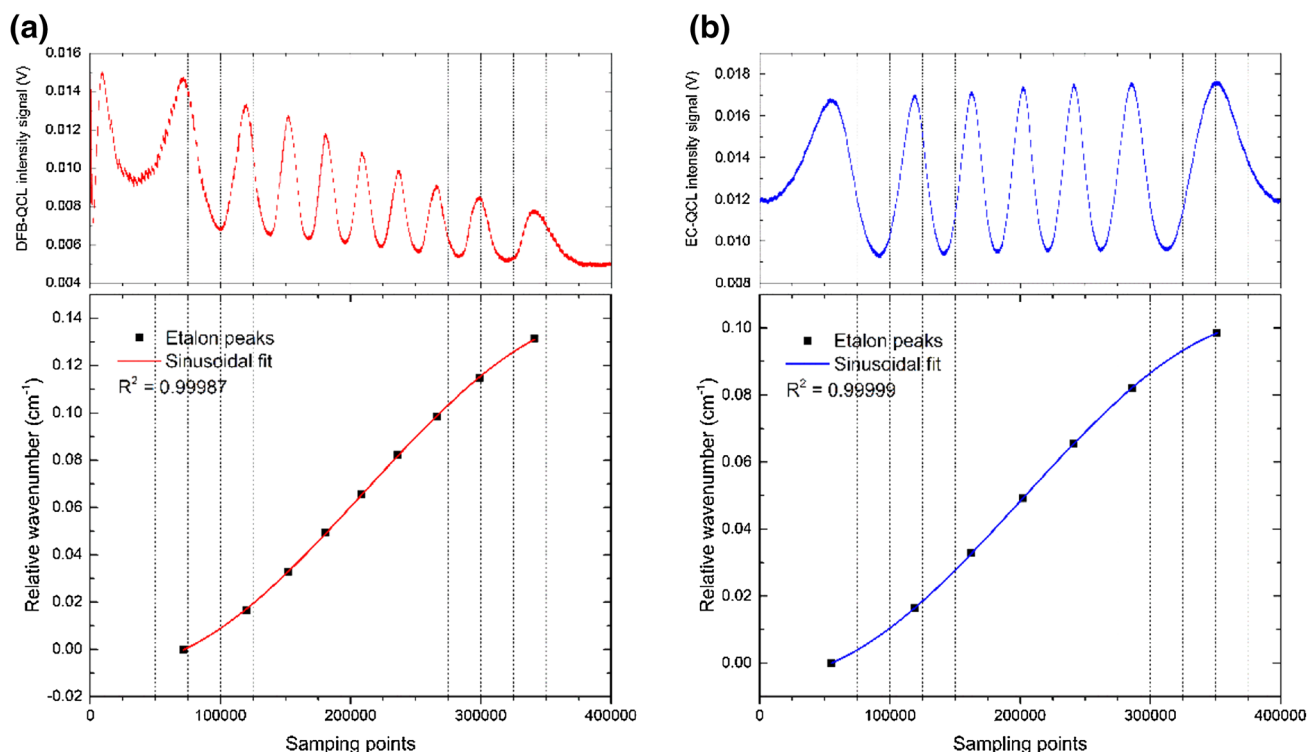
**Fig. 4** **a** DFB-QCL and **b** EC-QCL intensity signals through a germanium etalon (*upper panels*), and relative wavenumber variations fitted by sinusoidal functions (*lower panels*)
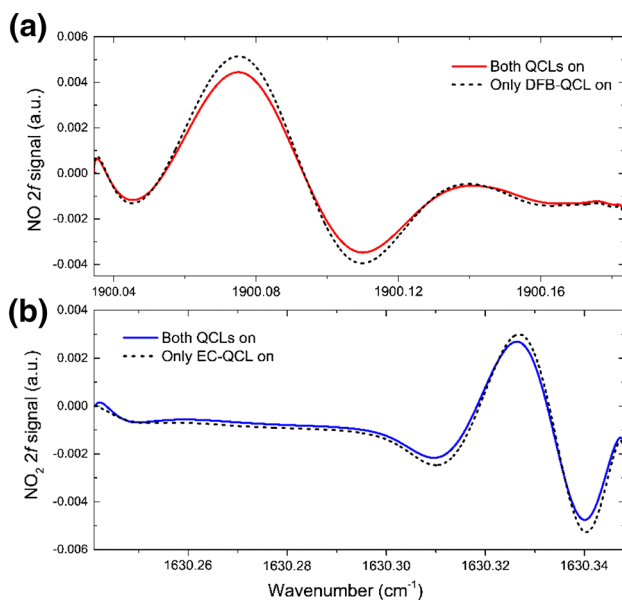


**Fig. 5** Comparison of the experimental 2*f* spectra of **a** NO when both QCLs were switched on (*red solid line*) and only DFB-QCL was switched on (*black dashed line*), and **b** NO₂ when both QCLs were switched on (*blue solid line*) and only EC-QCL was switched on (*black dashed line*)

# 3 Sensor performance

## 3.1 Characterization of WMDM-2*f* spectra

An example of experimental NO and NO₂ 2*f* spectra was recorded as shown in Fig. 5. NO and NO₂ were supplied into the sampling system by mixing the gases from two certified gas cylinders (1.01 ppmv NO:N₂ and 0.76 ppmv NO₂:N₂, respectively). The WMDM-2*f* spectra of NO (red solid line in Fig. 5a) and NO₂ (blue solid line in Fig. 5b) were obtained when both DFB-QCL and EC-QCL were switched on. The black dashed lines in Fig. 5a, b represent respective NO and NO₂ 2*f* signals of wavelength modulation spectroscopy (WMS) when only each corresponding QCL was switched on. The WMDM-2*f* and WMS-2*f* spectra have analogous profiles, between which a discrepancy, especially in the vicinity of the peak positions, is displayed due to the nonlinear detector responsivity. The nonlinear effect of the detector responsivity can be ignored when using WMDM for atmospheric NO$_x$ detection, because the absorption-induced power variation is small due to weak gas absorption features. The background 2*f* signals were non-zero

due to the nonlinear behavior of laser intensity modulation [13, 27, 29]. By comparing the simultaneous 2*f* spectra, no cross talk appeared to be associated with WMDM for the reported NO and NO$_2$ measurements. The peak amplitudes of WMDM-2*f* signals were acquired for the NO$_x$ concentration determination.

## 3.2 Modulation signal optimization

To optimize detection sensitivity of the NO$_x$ sensor system, an appropriate choice of modulation signals was required to maximize the WMDM-2*f* amplitudes of NO and NO$_2$. The amplitudes of NO and NO$_2$ WMDM-2*f* signals were recorded by modulating DFB-QCL and EC-QCL at different signals as plotted in Fig. 6, where NO and NO$_2$ concentration levels were fixed using the certified NO and NO$_2$ cylinders. According to the results in Fig. 6, a current of

12 mA and a voltage of 1.1 V were selected for DFB-QCL and EC-QCL modulation, respectively, for this study.

## 3.3 Sensitivity calibration

The linear response of the sensor system was investigated by measuring NO and NO$_2$ WMDM-2*f* signals at different mixing ratios. Different NO concentrations were generated by diluting the gas from the NO cylinder (1.01 ppm NO:N$_2$) with pure nitrogen (N$_2$) using a commercial gas dilution system (Environics, Series 4040). Because of its extremely strong oxidizability, no accurate NO$_2$ concentration can be proportionally produced through the gas dilution system. Therefore, the gas from the NO$_2$ cylinder (0.76 ppm NO$_2$:N$_2$) was mixed with another stream of pure N$_2$ at several different flow rates to obtain different NO$_2$ mixing ratios. Subsequently the concentration levels
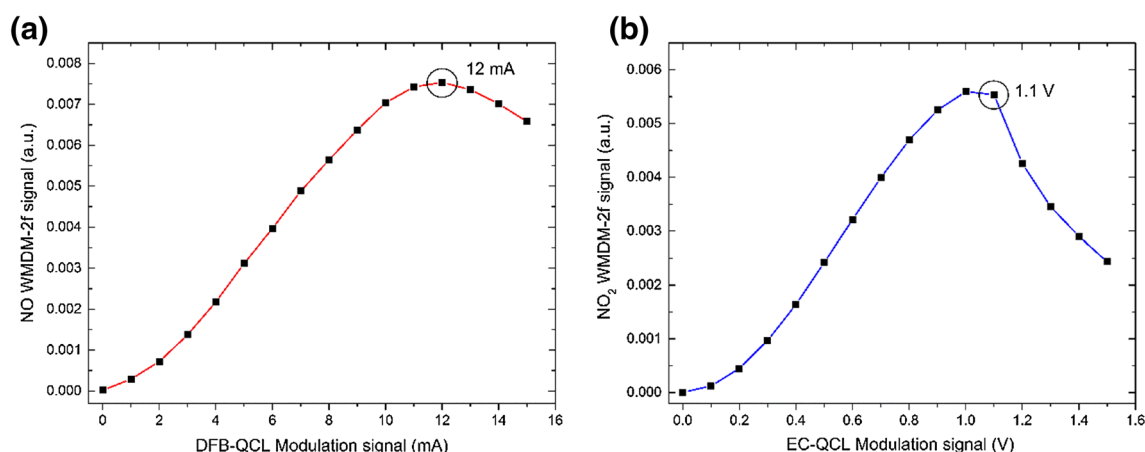


**Fig. 6** WMDM-2*f* amplitudes of **a** NO and **b** NO$_2$ at different DFB-QCL and EC-QCL modulation signals, respectively
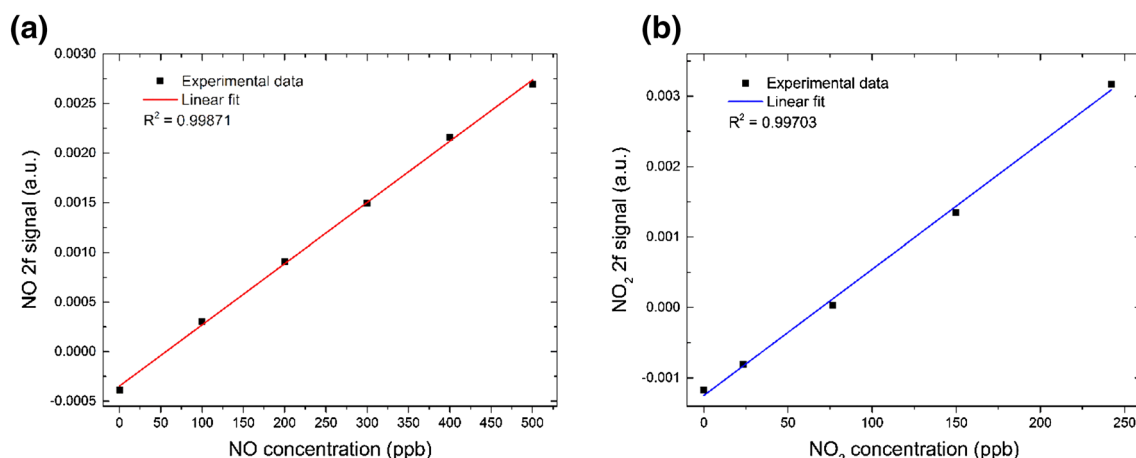


**Fig. 7** Measured WMDM-2*f* signals (*black square*) of **a** NO and **b** NO$_2$ as a function of respective gas concentrations. The *lines* were determined by least-squares linear regression

in the sampling system were calculated by least-squares fitting of the direct absorption curves to simulated Voigt profiles [30]. The NO and NO₂ WMDM-2*f* amplitudes were plotted as a function of respective concentrations and fitted by linear regression as depicted in Fig. 7. The coefficients of determination of these fittings are >0.997, indicating high stability and consistency of the NO$_x$ sensing system.

### 3.4 Noise level analysis

A noise level analysis of the reported WMDM-2*f* based sensor was implemented by flowing pure N₂ through the sampling system and recording the WMDM-2*f* signals in terms of NO and NO₂ concentrations during a 2.2-h period with 1-s time interval. An Allan–Werle variance method [31] was used to evaluate the long-term stability and precision of the sensor system, as shown in Fig. 8. Minimum detection limits (MDLs) of 2.45 ppbv for NO and 8.93 ppbv for NO₂ were achieved with a 1-s averaging time. Optimum MDLs were estimated to be 0.75 ppbv for NO and 0.9 ppbv for NO₂ with averaging times of 100 and 200 s, respectively, corresponding to detectable optical densities of $4.3 \times 10^{-5}$ and $3 \times 10^{-4}$. The decreasing dashed lines represent the theoretically expected $1/\sqrt{t}$ behavior of the sensor system dominated by the white noise prior to when the system drifts start to affect the sensor precision mainly due to flicker noise [32].

## 4 Conclusions

In conclusion, we have developed and demonstrated a dual QCL based sensor system dedicated to simultaneous NO and NO₂ detection. Two strong absorption lines of NO at 1900.075 cm$^{-1}$ and NO₂ at 1630.33 cm$^{-1}$ were identified and selected for interference-free concentration measurements. A wavelength modulation-division multiplexing technique along with LabView-based data analyzers was implemented to realize the simultaneous detection with a large spectral interval of ~270 cm$^{-1}$. The performance of the sensor system, characterized by Allan–Werle variance



**Fig. 8** Allan deviation plots of **a** NO (in *red*) and **b** NO₂ (in *blue*) concentrations as a function of averaging time
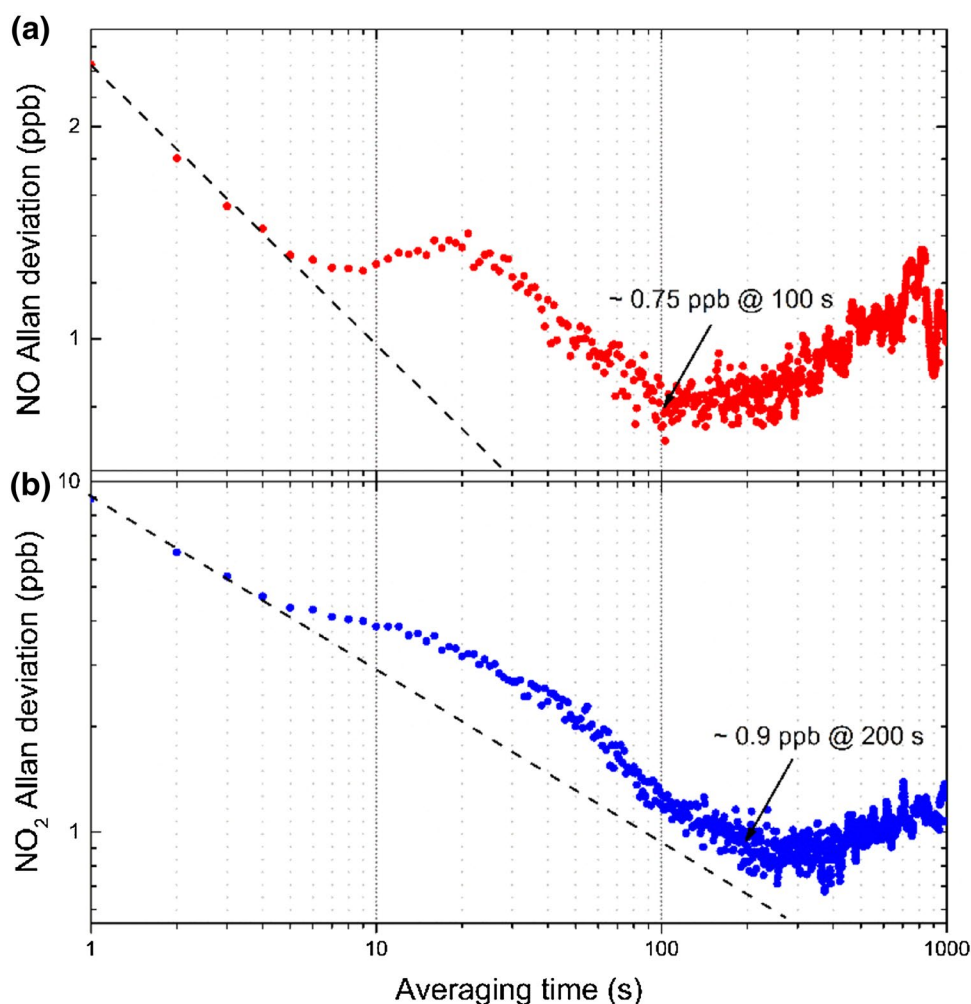
analysis, was assessed and yielded MDLs of 2.45 ppbv for NO and 8.93 ppbv for $NO_2$ with a 1-s averaging time. This analysis indicated that the MDLs can be improved to be 0.75 ppbv for NO and 0.9 ppbv for $NO_2$ with averaging times of 100 and 200 s, respectively, which are sensitive enough to quantify $NO_x$ concentrations at atmospheric levels. This sensor system can be readily adapted for simultaneous detection of additional gas species by including appropriate laser sources operating at different modulation frequencies.

# References

1. P.J. Crutzen, Annu. Rev. Earth Planet. Sci. **7**, 443 (1979)
2. J.A. Logan, J. Geophys. Res. **88**, 10785 (1983)
3. P.L. Kebabian, S.C. Herndon, A. Freedman, Anal. Chem. **77**, 724 (2005)
4. A. Karpf, G.N. Rao, Appl. Opt. **48**, 408 (2009)
5. P.V. Hobbs, *Introduction to Atmospheric Chemistry* (Cambridge University Press, New York, 2000), p. 160
6. K. Liu, R. Lewicki, F.K. Tittel, Sens. Actuators B **237**, 887 (2016)
7. I.B. Pollack, B.M. Lerner, T.B. Ryerson, J. Atmos. Chem. **65**, 111 (2010)
8. B. Tuzson, K. Zeyer, M. Steinbacher, J. McManus, D. Nelson, M. Zahniser, L. Emmenegger, Atmos. Meas. Tech. **6**, 927 (2013)
9. C. Reed, M.J. Evans, P.D. Carlo, J.D. Lee, L.J. Carpenter, Atmos. Chem. Phys. **16**, 4707 (2016)
10. J.L. Jimenez, G.J. McRae, D.D. Nelson, M.S. Zahniser, C.E. Kolb, Environ. Sci. Technol. **34**, 2380 (2000)
11. B.A. Mann, R.F. White, R.J. Morrison, Appl. Opt. **35**, 475 (1996)
12. X. Chao, J.B. Jeffries, R.K. Hanson, Proc. Combust. Inst. **33**, 725 (2011)
13. X. Chao, J. Jeffries, R. Hanson, Appl. Phys. B **106**, 987 (2012)
14. G. Wysocki, A. Kosterev, F. Tittel, Appl. Phys. B **80**, 617 (2005)
15. D. Nelson, J. Shorter, J. McManus, M. Zahniser, Appl. Phys. B **75**, 343 (2002)
16. R. Curl, F. Tittel, Annu. Rep. Sect. C (Phys. Chem). **98**, 219 (2002)
17. Y.A. Bakhirkin, A. Kosterev, R. Curl, F. Tittel, D. Yarekha, L. Hvozdara, M. Giovannini, J. Faist, Appl. Phys. B **82**, 149 (2006)
18. A.A. Kosterev, A.L. Malinovsky, F.K. Tittel, C. Gmachl, F. Capasso, D.L. Sivco, J.N. Baillargeon, A.L. Hutchinson, A.Y. Cho, Appl. Opt. **40**, 5522 (2001)
19. I. Courtillot, J. Morville, V. Motto-Ros, D. Romanini, Appl. Phys. B **85**, 407 (2006)
20. M.I. Mazurenka, B.L. Fawcett, J.M. Elks, D.E. Shallcross, A.J. Orr-Ewing, Chem. Phys. Lett. **367**, 1 (2003)
21. R. Wada, A.J. Orr-Ewing, Analyst **130**, 1595 (2005)
22. H. Fuchs, W.P. Dubé, B.M. Lerner, N.L. Wagner, E.J. Williams, S.S. Brown, Environ. Sci. Technol. **43**, 7831 (2009)
23. J. Jágerská, P. Jouy, B. Tuzson, H. Looser, M. Mangold, P. Soltic, A. Hugi, R. Brönnimann, J. Faist, L. Emmenegger, Opt. Express **23**, 1512 (2015)
24. D.B. Oh, M.E. Paige, D.S. Bomse, Appl. Opt. **37**, 2499 (1998)
25. G. Wysocki, R.F. Curl, F.K. Tittel, R. Maulini, J.-M. Bulliard, J. Faist, Appl. Phys. B **81**, 769 (2005)
26. G. Wysocki, R. Lewicki, R. Curl, F. Tittel, L. Diehl, F. Capasso, M. Troccoli, G. Hofler, D. Bour, S. Corzine, Appl. Phys. B **92**, 305 (2008)
27. Y. Yu, N.P. Sanchez, R.J. Griffin, F.K. Tittel, Opt. Express **24**, 10391 (2016)
28. L.S. Rothman, I.E. Gordon, Y. Babikov, A. Barbe, D.C. Benner, P.F. Bernath, M. Birk, L. Bizzocchi, V. Boudon, L.R. Brown, J. Quant. Spectrosc. Radiat. Transf. **130**, 4 (2013)
29. H. Li, G.B. Rieker, X. Liu, J.B. Jeffries, R.K. Hanson, Appl. Opt. **45**, 1052 (2006)
30. D. Rehle, D. Leleux, M. Erdelyi, F. Tittel, M. Fraser, S. Friedfeld, Appl. Phys. B **72**, 947 (2001)
31. P. Werle, R. Mücke, F. Slemr, Appl. Phys. B **57**, 131 (1993)
32. P. Werle, Appl. Phys. B **102**, 313 (2011)